Research Article

Arianit A. Reka*, Blagoj Pavlovski, Emira Fazlija, Avni Berisha, Musaj Pacarizi, Maria Daghmehchi, Carmen Sacalis, Gligor Jovanovski, Petre Makreski, Ayhan Oral

Diatomaceous Earth: Characterization, thermal modification, and application

https://doi.org/10.1515/chem-2020-0049
received March 26, 2020; accepted March 4, 2021

Abstract: The diatomaceous earth (DE), collected from the Mariovo region in North Macedonia, was characterized and thermally modified. The material represents a sedimentary rock of biogenic origin, soft solid that can be easily disintegrated, with white to grayish color, with bulk density of 0.51–0.55 g/cm^3, total porosity of 61–63%, and specific gravity of 2.25 g/cm^3. The chemical composition is as follows: SiO_2, 86.03; Al_2O_3, 3.01; Fe_2O_3, 2.89; MnO, 0.06; TiO_2, 0.20; CaO, 0.76; MgO, 0.28; K_2O, 0.69; Na_2O, 0.19; P_2O_5, 0.15; and loss of ignition, 5.66 (wt%). The mineralogy of the raw DE is characterized by the predominant presence of amorphous phase, followed by crystalline quartz, muscovite, kaolinite, and feldspar. Significant changes in the opal phase are observed in the 1,000–1,200°C temperature region. At 1,100°C, the entire opal underwent solid–solid transition to cristobalite. Further ramp of the temperature (1,100–1,200°C) induced formation of mullite. Scanning electron microscopy (SEM) and transmission electron microscopy depict the presence of micro- and nanostructures with pores varying from 260 to 650 nm. SEM analysis further determined morphological changes in terms of the pore diameters shrinkage to 120–250 nm in comparison to the larger pores found in the initial material. The results from this investigation improve the understanding of mechanism of silica phase transition and the relevant phase alterations that took place in DE upon calcination temperatures from 500 to 1,200°C.

Keywords: diatomaceous earth, calcination, thermal modification, natural nanomaterial

*** Corresponding author: Arianit A. Reka,** Department of Chemistry, Faculty of Natural Sciences and Mathematics, University of Tetovo, Bldv. Ilinden n.n., 1200 Tetovo, Republic of North Macedonia; NanoAlb, Albanian Unit of Nanoscience and Nanotechnology, Academy of Sciences of Albania, Fan Noli square, 1000 Tirana, Albania, e-mail: arianit.reka@unite.edu.mk
Blagoj Pavlovski: Institute of Inorganic Technology, Faculty of Technology and Metallurgy, Ss. Cyril and Methodius University, Ruger Boskovic n.n., 1000 Skopje, Republic of North Macedonia
Emira Fazlija: Department of Chemistry, Faculty of Natural Sciences and Mathematics, University of Tetovo, Bldv. Ilinden n.n., 1200 Tetovo, Republic of North Macedonia
Avni Berisha, Musaj Pacarizi: NanoAlb, Albanian Unit of Nanoscience and Nanotechnology, Academy of Sciences of Albania, Fan Noli square, 1000 Tirana, Albania; Department of Chemistry, Faculty of Natural Sciences and Mathematics, University of Pristina "Hasan Prishtina", 10000 Pristina, Republic of Kosovo
Maria Daghmehchi: Department of Archaeology, University of Tehran, Tehran 6619-14155, Iran
Carmen Sacalis: Department of Chemistry, Faculty of Chemistry and Chemical Engineering, Babes-Bolyai University, 11 Arany Janos St., 400028 Cluj-Napoca, Romania
Gligor Jovanovski: Research Center for Environment and Materials, Academy of Sciences and Arts of North Macedonia, MASA, Bul. Krste Misirkov 2, 1000 Skopje, North Macedonia
Petre Makreski: Institute of Chemistry, Faculty of Natural Sciences and Mathematics, Ss. Cyril and Methodius University, Arhimedova 5, 1000 Skopje, Republic of North Macedonia
Ayhan Oral: Department of Materials Science and Engineering, Çanakkale Onsekiz Mart University, Campus of Terzioglu, 17100 Çanakkale, Turkey

1 Introduction

Diatomaceous earth (DE, otherwise known as diatomite) is a very important natural material used in industry comprising distinctive combinations of physical and chemical properties. Typically, it is a soft, friable, fine-grained, weakly cemented, porous, and light-weight sedimentary siliceous rock. Other valuable characteristics of DE are low bulk density, low thermal conductivity, inert chemical reactivity with most liquids and gases, and sparingly solubility in water. These properties classify DE as a very attractive natural material with distinctive properties, i.e., high permeability, high porosity, and large surface area. Depending on the amount of present impurities, its color varies from white to yellowish gray, dark gray, and brownish-gray [1–5]. DE is considered to be a natural nanomaterial [6], composed mainly of accumulated remains of skeletons [7]. DE has a variety of uses and applications such as obtaining humidity control materials [8], material for filtration [9], raw material

for production of cement [10], initial material for production of prolonged-release drug carriers [11], sorption, desorption and industrial scale absorption material [12–14], production of porous ceramics [15–17], glass industry [18,19], catalyst support [20], filler in paints and plastics [21], purification of industrial waters [22], pozzolanic material, pesticide holder, and also as a material for improving the physical and chemical characteristics of certain soils, etc. [22–28].

The excavated DE from geological deposits may contain diverse metal oxides and organic matter associated with the dominant silica content (SiO_2). The most abundant association involves Al_2O_3, Fe_2O_3, CaO, MgO, K_2O, Na_2O, and P_2O_5 that might be even beneficial toward its application properties [29]. One way to improve the properties of DE is through calcination process that facilitates the removal of impurities from the frustules resulting in improvement of the DE industrial quality [30–34].

The USA was the main producer of DE in 2019, accounting for an approximate 34% of its world production, accompanied by China and Denmark with 15% each, Turkey with 6%, Republic of Korea 5%, Peru 4%, and Mexico with 3%. Smaller quantities of DE were mined in 23 other countries [35]. North Macedonia fits in this group being rich in DE and other silica-based materials (trepel, perlite, pumice, etc.) [36–42] with a wide scope of potential utilization and application. The economic benefit of using DE from North Macedonia is based on its fine microstructure and, more importantly, because of the presence of non-crystalline (amorphous) phase. Such characteristics make this material distinctly reactive. The determination of the mineralogical alterations that arise during the thermal treatment process of DE is of a great significance that will govern its further use and application in various technological processes. Thus, the aim of this research was to monitor the effect of the calcination on the silica phase transformation along with determining the temperature at which it remains amorphous. Despite the thermal behavior of the DE, particular interest was stressed to follow up the changes that occurred in the frustules. The transition mechanisms of the occurring phenomena were followed by the synergistic use of structural, thermal, microscopy, and spectroscopy techniques.

2 Materials and methods

The raw DE used in this study was collected from the Mariovo area, North Macedonia [43].

The chemical composition of natural DE was determined using the classical chemical analysis (for silicates). DE was fused in a mixture of carbonates, while the percentages of other oxides found in the material were determined by complexometric titration. The presence of Na_2O and K_2O was determined by flame atomic emission spectroscopy. The trace elements were determined using ICP-MS (Agilent 7500cx).

The determination of the mineralogical content of DE was performed using X-ray powder diffraction (XRPD), thermal analysis (thermogravimetric/differential thermal analysis [TGA/DTA]), and scanning electron microscopy (SEM-EDX). XRPD analysis was carried out on Rigaku Ultima IV X-ray diffractometer set-up with D/teX high-speed 1-dimensional detector, using CuKα radiation (λ = 1.54178 Å) in the range from 5 to 60°C. The accelerating voltage was set at 40 kV, while the current power was set at 40 mA.

The Perkin-Elmer FTIR system 2000 interferometer was engaged to record the infrared spectra in the 4,000–450 cm^{-1} spectral region using the KBr pellet method. The pellet was prepared by loading pressure (10 tons) onto a solid mixture of 1 mg of sample with 250 mg of dried KBr.

The thermal analyses (DTA/TGA) of the raw DE were carried out in air conditions using a Universal V4.5A TA Instrument, SDT Q600 V20.9 Build 20 apparatus, under the following experimental set-up: temperature span of 20–1,200°C; rate of heating of 10°C/min and a thermal treatment duration time of 108 min; and mass of sample of 10 mg, with a ceramic pot as a carrier for the material.

SEM VEGA3 LMU coupled with energy-dispersive X-ray spectroscopy (INCA Energy 250 Microanalysis System) was used to quantitatively examine the material. The accelerating voltage of the SE detector was set to 20 kV.

Transmission electron microscopy (TEM) on the natural DE was performed using Hitachi H-7650 instrument (120 kV automatic microscope).

For the purpose of the thermal investigations, raw DE was calcined ramping the temperature from 500 to 1,200°C with a duration of 1 h and 100°C between each step.

Ethical approval: The conducted research is not related to either human or animal use.

3 Results and discussion

3.1 Physicomechanical properties of the DE

From the physicomechanical perspective, the tested DE (Figure 1) represents a very light and soft (1–2 Mohs)

Figure 1: Natural (crude) DE from Mariovo.

sedimentary rock of biogenic origin white in color. It represents a fine-superfine grained structure, porous (61–63%), with a shell-like fragility, and sticks to the tongue. No obvious reaction with HCl was observed. The bulk density of DE is 0.51–0.55 g/cm^3, and the density is 2.25 g/cm^3, while the compressive strength in its natural state (raw) is 7.67 MPa.

3.2 Chemical analysis of the DE

The chemical composition of DE (Table 1) was determined using the classical chemical analysis (for silicates). The loss of ignition (LOI), determined during heating the natural DE at 1,000°C for a duration of 1 h, was 5.66%. The results acquired from the chemical composition of DE indicate that the tested material constitutes an acidic rock with predominating percentage of SiO_2 (86.03%) and relatively low content of Al_2O_3 (3.01%) and Fe_2O_3 (2.89%) with the content of each of the remaining oxides remains below 1% (Table 1).

The content of the trace elements (Table 2) revealed abundance of Cu, Cr, V, Rb, Sr, Cs, and Mo in the 30–100 ppm range, whereas the major presence was found for Ba (165 ppm), U (249 ppm), and As (586 ppm). The significant content of U is explained by the existence of the U-bearing zones and minerals in the Mariovo region [44,45]. The relatively high content of As could be related to the high presence of arsenic ores and the very abundant arsenic mineralization particularly typical for the nearby site of Allchar. Namely, the famous Allchar mine as a part of the Kozhuf volcanic area and as the youngest volcanic area lies only around 10 km east from the Mariovo-Kajmakčalan volcanic area that stretches between the Nidže Mountain with Kajmakčalan in the south and the village of Vitolište in the north being in the vicinity of the examined DE locality [43]. The content of the remaining trace elements is very low, not exceeding 10 ppm.

3.3 XRPD analysis of DE

The X-ray diffractogram of DE (Figure 2) mainly represents the amorphous phase with a minor presence of crystalline phases. The manifestation of the wide "bump" positioned between 15° and 28° (2θ) is ascribed to the existence of opal in the sample.

The crystalline phases evident in the sample are as a result of quartz, SiO_2 (peaks *d* 4.25 at 20.88°; *d* 3.34 at 26.66°; *d* 2.27 at 39.51°; *d* 1.81 at 50.16°; *d* 1.54 Å at 59.58° 2θ); muscovite, $KAl_2(Si_3Al)O_{10}(OH,F)_2$ (*d* 9.91 at 8.91°; *d* 4.96 at 17.85°; *d* 4.48 at 19.76°; *d* 3.31 at 26.90°; *d* 2.98 at 29.89°; *d* 2.80 at 31.85°; *d* 2.59 at 34.51°; *d* 2.35 at 38.19°; *d* 2.14 at 42.15°; *d* 1.99 at 45.59°; *d* 1.97 at 45.94°; *d* 1.74 at 52.54°; *d* 1.65 Å at 55.53° 2θ); kaolinite, $Al_2Si_2O_5(OH)_4$ (*d* 3.58 at 24.79°; *d* 7.18 at 12.36°; *d* 1.65 at 55.44°; *d* 2.33 at 38.84°; *d* 2.55 Å at 35.05° 2θ); and plagioclase feldspars, $NaAlSi_3O_8$–$CaAl_2Si_2O_8$ (*d* 3.25 at 27.42°; *d* 3.77 at 23.55°; *d* 4.02 at 22.10°; *d* 3.19 at 27.86°; *d* 3.60 Å at 24.68° 2θ) [46,47].

3.4 Infrared spectra analysis of DE

The FTIR spectrum (Figure 3) of the DE displays a very strong absorption band at 1,100 cm^{-1} with an associated shoulder at 1,250 cm^{-1} that are attributed to the antisymmetric stretching Si–O vibrations. The absorption band at 800 cm^{-1} evolves from the corresponding symmetric extension–compression vibration of Si–O [48–50]. The bands at 469, 532, and 695 cm^{-1} fingerprint the presence of muscovite [51], whereas the weak absorption bands at

Table 1: Chemical composition of the DE

Oxide	SiO_2	Al_2O_3	Fe_2O_3	MnO	TiO_2	CaO	MgO	K_2O	Na_2O	P_2O_5	LOI	Total
Mass%	86.03	3.01	2.89	0.06	0.20	0.76	0.28	0.69	0.19	0.15	5.66	99.92

Table 2: Content of trace elements found in DE

Element	ppm	Element	ppm	Element	Ppm	Element	ppm
Cu	97	Cd	0.076	Sr	87.8	Pd	4.1
Cr	33.0	As	586.4	Cs	35.0	Ag	1.2
Ni	9.0	Se	1.1	Th	7.9	Ga	6.8
Co	3.2	Tl	6.88	U	248.7	Ge	0.6
Zn	1.22	Bi	0.41	Mo	42.4	Li	11.64
V	56.7	Ba	165.4	Sn	1.1	Be	1.2
Pb	8.9	Rb	45.3	Sb	0.4	B	<10

913, 3,621, and 3,696 cm^{-1} originate from the present kaolinite [51–54]. The broad band at ~3,430 cm^{-1} is because of the H–O–H stretching vibrations of absorbed water, while the band at 1,639 cm^{-1} is attributed to the presence of opal in the sample and is because of the H–O–H bending vibrations from the absorbed water in opal.

3.5 Thermally induced study of DE

TGA along with DTA of the tested specimen were undertaken because the response of the material upon heating is of great importance to determine its technological properties (Figure 4).

The results from the TG analysis inferred that weight loss took place in three temperature intervals. The first temperature span extends from room temperature to 265°C exhibiting weight loss of 8.07% that is attributed to the elimination of adsorbed and absorbed water in DE. The second temperature interval spans between 265 and 600°C are characterized by weight loss of 3.26% being attributed to the dehydration process of the chemically bonded water in opal structure and burning of the organic matter existing in diatomite [53]. The third temperature interval (from 600 to 1,100°C) followed by the minor weight loss of 2% is ascribed to the dehydroxylation of the clay constituents (muscovite and kaolinite) [54,55].

3.6 SEM of DE

The results from the SEM (Figure 5) revealed the biogenic identity of the raw DE. Namely, various frustules and/or entire skeletal structures of diatoms algae (most of the time in the shape of sunflowers) ranging from 5 to 15 μm were registered. SEM morphology of DE indicates the presence of preserved forms of the diatom frustules. The existence of other shapes, which are in all probability as a result of the clay constituent in the material, is also evident. The size of the pores ranges between 200 and 460 nm in diameter.

The EDX spectrum facilitated into the quantitative determination of the chemical content of the analyzed

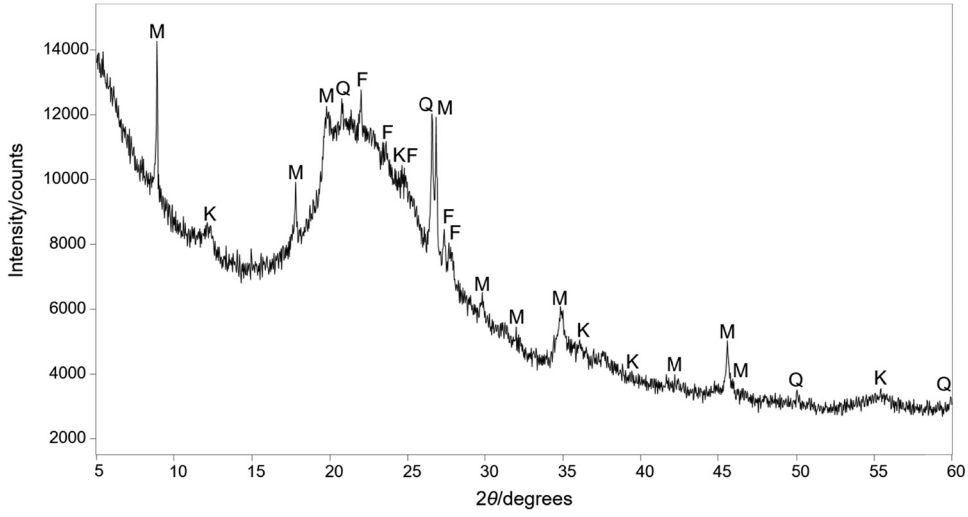

Figure 2: XRPD pattern of the raw DE. The strongest peaks arising from muscovite (M), kaolinite (K), quartz (Q), and feldspars (F) are marked.

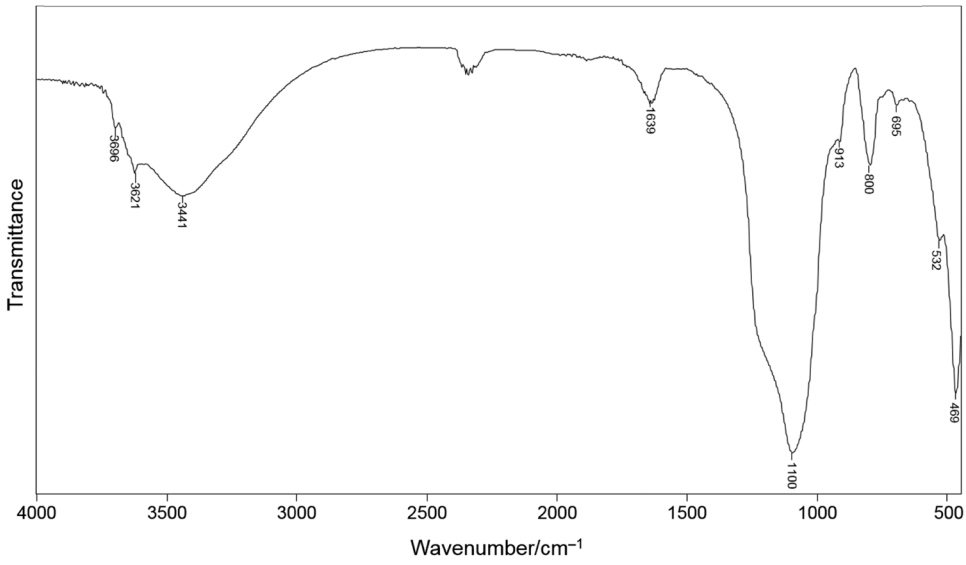

Figure 3: FTIR spectrum of the DE.

sample (Figure 6a) and confirmed the purity of skeletons being actually majorly composed of silica, SiO_2 (O: 70.03% and Si: 29.97%). However, the surplus deviation of the oxygen content from the ideal SiO_2 stoichiometry is incorporated in the calculation of the chemical formulae (Figure 6b, O: 64.65%, Al: 3.16%, Si: 30.20%, K: 0.69%, and Fe: 1.30%) of the other associated clay minerals that evolve from the associated clayey minerals within the sample (muscovite and kaolinite).

3.7 TEM of the natural diatomite

The results from the TEM (Figure 7) were complementary with SEM analysis regarding the texture and the morphology of the raw material. A heterogeneous population constituted by morphologically size-different nanostructures was observed. The results from the TEM analysis of the DE indicated mainly glassy features (Figure 7), resulting from the amorphous phase in the material.

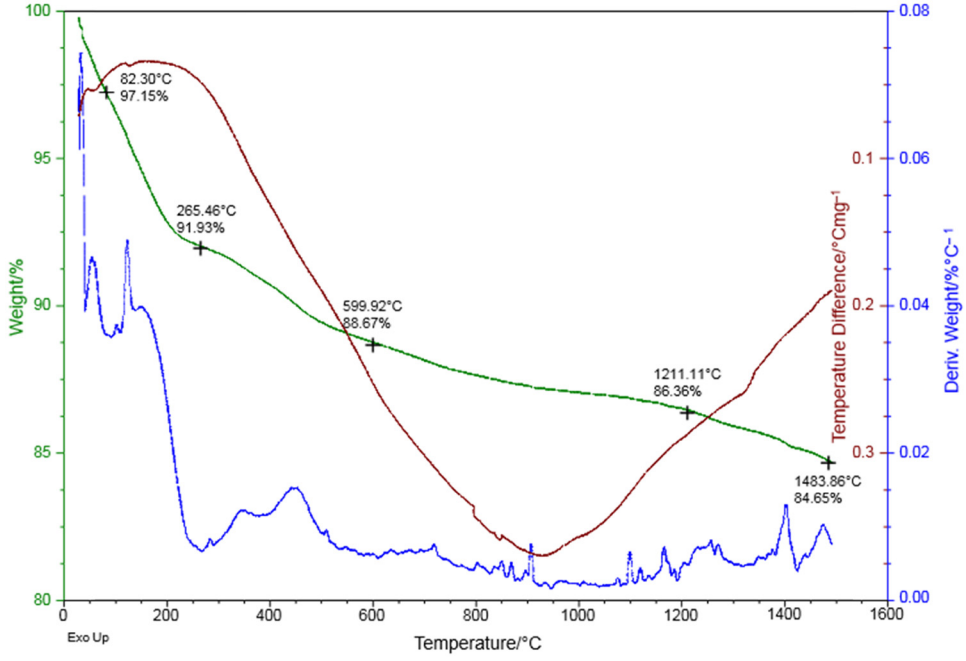

Figure 4: TG/DT analysis of DE.

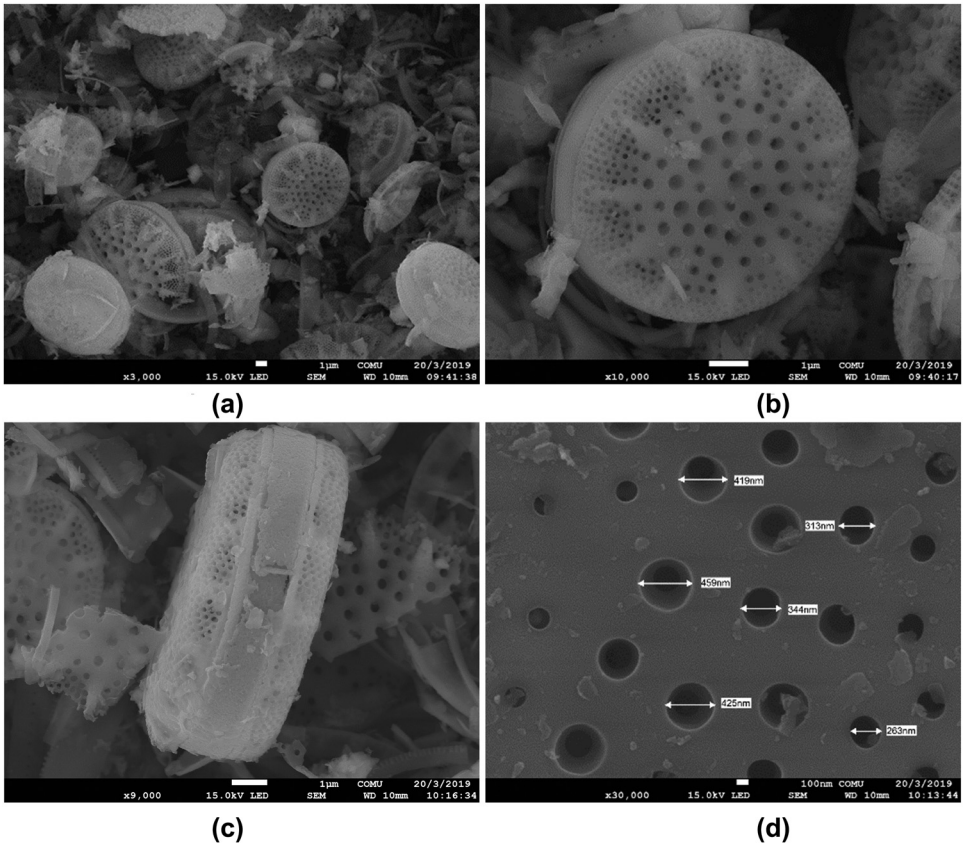

Figure 5: SEM examination of raw DE. (a) Several valves of *Tertiarius jurijlii* and probably one frustule of *T. mariovensis* in right bottom corner, (b) a whole valve of *T. jurijlii*, (c) *T. jurijlii* girdle view, and (d) Areolae in the central area of *T. jurijlii* [56].

The diatom shells in DE exhibit rich porous structure and uncontaminated surface, while the impurities observed inside the nanometric pores were, most likely, related to the association of clayey minerals [57]. In comparison to other nanocarriers, the nanometric proportions and morphology of structures found in the DE positioned the material as a suitable candidate for use in drug delivery applications [58].

3.8 XRPD examination of the calcined DE

Results from the XRPD examination of the thermally induced DE at 500, 600, 700, 800, 900, 1,000, 1,100, and 1,200°C (Figure 8) revealed the presence of opal in the temperature interval 500–1,000°C explained by complex halo peak (typical for any amorphous phase) between 19° and 25° (2θ) [47]. On the contrary, significant alteration of the opal phase was observed in the temperature interval 1,000–1,100°C with the entire opal component underwent solid–solid transition to cristobalite that remained unaffected at 1,200°C.

The muscovite phase was registered in thermal steps until 900°C, whereupon its complete disintegration was observed [59].

The XRPD results also pointed out on the existence of quartz phase up to 1,000°C whose presence is diminished at higher temperatures evidenced by the severe intensity reduction in the corresponding peaks at *d*-values of 3.34, 4.26, and 1.81 Å (2θ angles at 26.66°, 20.83°, and 50.37°). At 1,100°C, crystallization of opal into cristobalite occurs, and at the same time transformation of quartz into cristobalite also occurs. No presence of quartz was evidenced at the highest calcined temperature of 1,200°C.

XRPD pattern of the calcined DE at 1,000°C showed minimal intensity of peaks resulting from the mullite phase, $Al_6Si_2O_{13}$. Further temperature increase at 1,100°C resulted in the appearance of all mullite characteristic maxima at *d*-values of 5.40, 3.44, 3.40, 2.69, 2.55, and 2.22 Å (2θ angles at 16.40°, 25.87°, 26.18°, 33.28°, 35.16°, and 40.60°) that remained practically unchanged at the highest ramped temperature of 1,200°C [46,47].

The kinetics and the mechanism of transformation of opal in the DE mainly depend on the purity of the

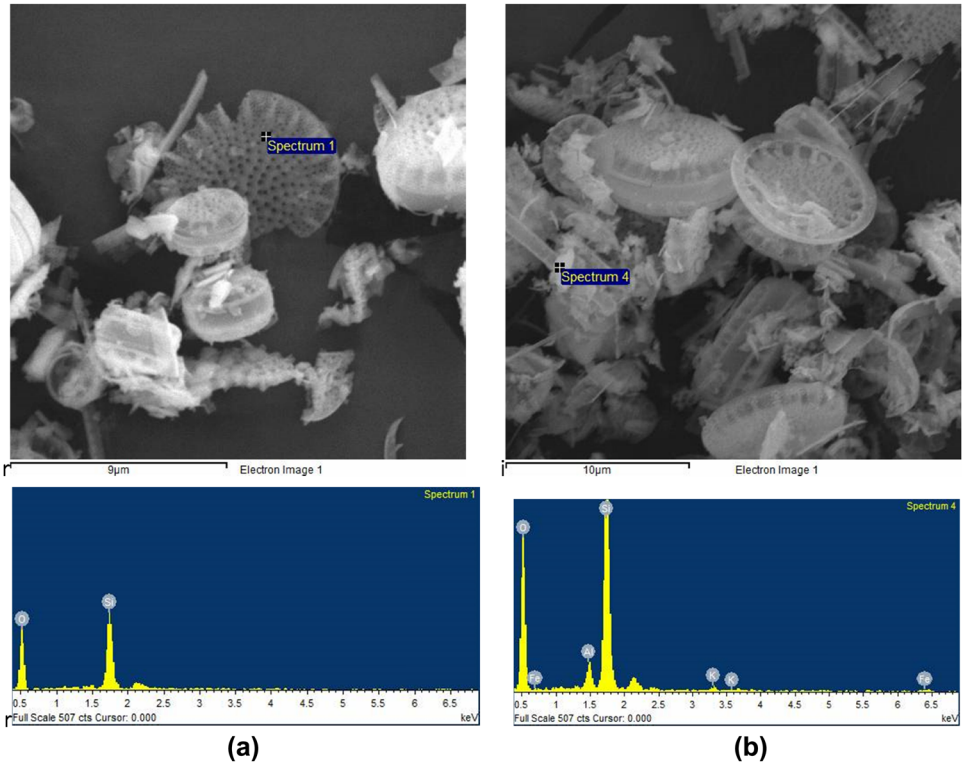

Figure 6: SEM/EDX analysis of the skeletons (a) and the associate clayey minerals (b) found in DE.

material itself. The DE with higher percent of SiO_2 (92.97 wt%) calcined in powder state at a temperature of 1,100°C in an interval of 1 and 2 h remains amorphous. The same DE during heating at 1,200°C in an interval of 1 and 2 h underwent partial crystallization of opal into quartz and cristobalite. The sample calcined at 1,200°C for 2 h shows increase in the cristobalite phase associated with a decrease in the content of the quartz phase. This result indicates that the crystallization of the amorphous SiO_2 to cristobalite goes through the quartz phase [31]. This shows that the impurities in the analyzed DE act toward lowering of the crystallization temperature of opal into cristobalite for about 100°C.

3.9 SEM of the calcined DE

SEM examinations were also conducted in the calcined regime (500–1,200°C), with no significant changes observed until 900°C. However, further ramp of the temperature at 1,000, 1,100, and 1,200°C for an interval of 1 h (Figure 9)

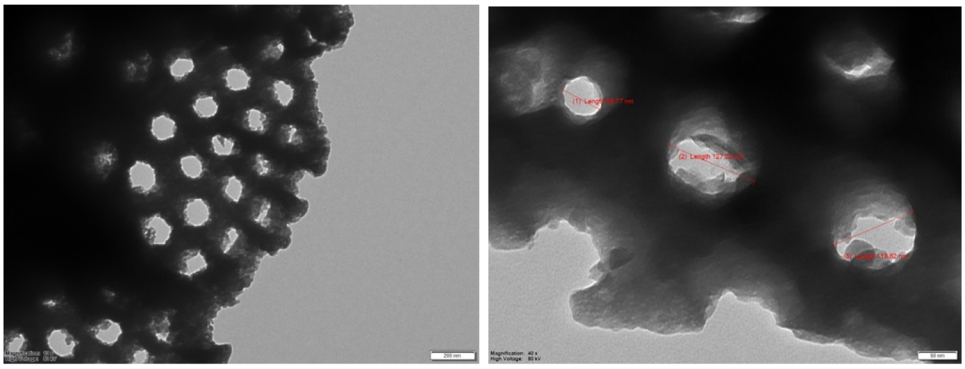

Figure 7: TEM analysis of natural DE.

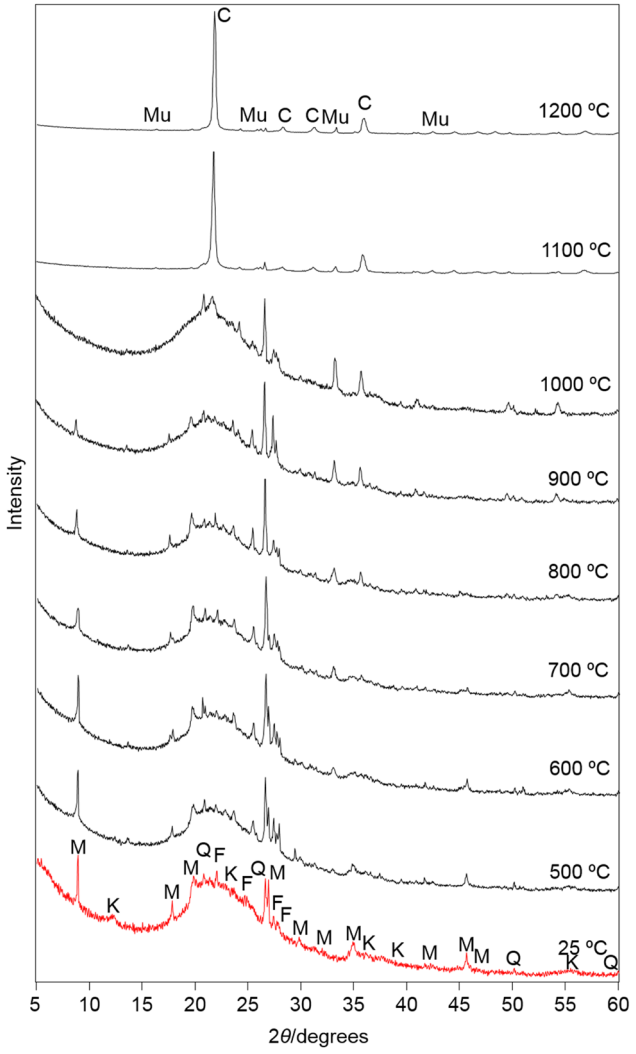

Figure 8: XRPD analysis of the starting and the series of the calcined DE in the 500–1,200°C range. The evolution of the peaks from mullite (Mu) and cristobalite (C) at the 1,100 and 1,200°C diagrams is marked. The peaks from muscovite (M), kaolinite (K), quartz (Q), and feldspars (F) in the starting material are also denoted.

generated different morphology in the surface texture, pore dimensions, and form. Namely, the average pore dimensions of the calcined DE decreased while ramping the temperature from 1,000 to 1,200°C (Figure 9). The abrupt shrinkage was evidenced at 1,200°C when some of the diatomite pores completely annihilated and disappeared. Such observation was mainly attributed to the impurities (causing fusion during calcination) in the DE that promote the eutectics formation at lower temperatures. The SEM observation is neatly supporting the XRPD results for transformation of opal into cristobalite (1,000–1,200°C) in terms of agglomeration of the particles resulting in the decrease in the pore size that lowered the total porosity.

4 Conclusion

The physical–mechanical characteristics revealed that the DE from Mariovo represents white, soft material with a low bulk density and high porosity. The mineralogical composition showed predominantly the amorphous phase with a small fraction of crystalline phases. The amorphous phase is attributed to the amorphous opal of biogenic origin (frustules), while the crystalline phases mainly consist of quartz and clay minerals mostly pronounced by dominant muscovite followed by kaolinite. Microscopic SEM and TEM examinations demonstrate an existence of micro- and nanostructures with pores ranging from 250 to 650 nm. The conducted calcination experiment helped to resolve and understand the silica phase transition and the relevant phase alterations that took place. During the calcination process of the DE, the amorphous opal transformed into cristobalite (not to tridymite) as a result of the aggregation of

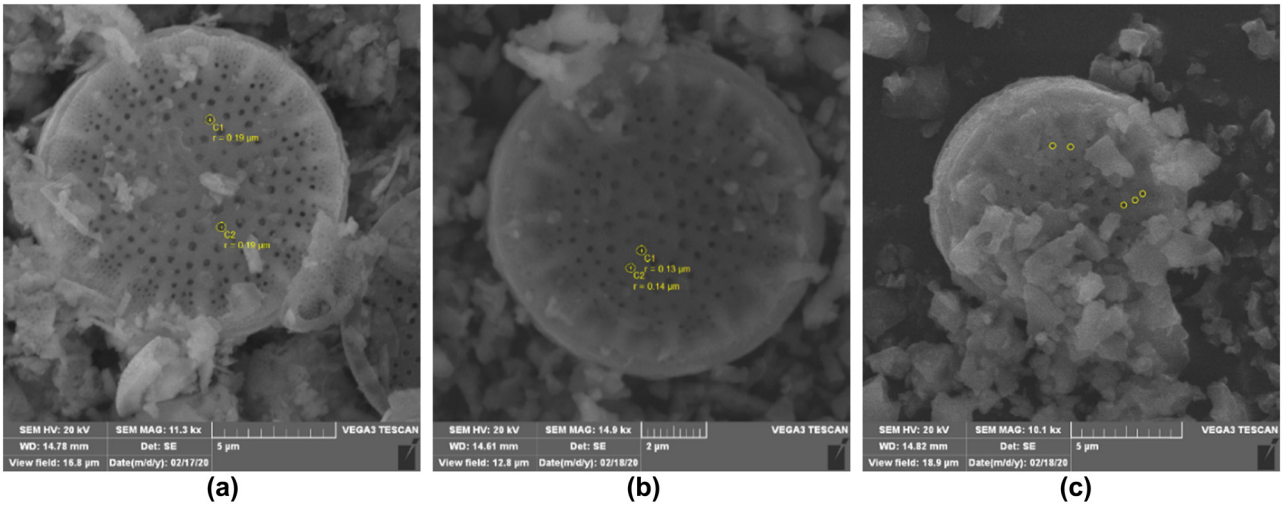

Figure 9: SEM analysis of calcined DE, calcined for 60 min: (a) at 1,000°C, the average pore size 380–400 nm; (b) at 1,100°C, average pore size 260–280 nm; and (c) at 1,200°C, average pore size 120–250 nm.

microcrystalline cristobalite in the amorphous opal. Significant changes in the opal phase were observed in the temperature interval 1,000–1,100°C. Based on the debayegram of the calcined DE at 1,100°C, it can be observed that the entire opal underwent total solid–solid phase transformation to cristobalite. SEM examinations revealed that during the transformation temperature of opal, an agglomeration of the nano-sized opal and particle growth took place, which was correlated with the decrease in the porosity and specific surface of the obtained cristobalite. The obtained cristobalite remained stable at 1,200°C. The type and the amount of the impurities (clay minerals and feldspars) contribute to the lowering of the crystallization temperature of the opal component into cristobalite for about 100°C. Moreover, the temperature interval 1,100–1,200°C depicted the formation of mullite. Having in mind the mullite affects both physical and mechanical characteristics of ceramics by increasing their shock resistance along with mechanical strength, the studied DE from Mariovo stands as a material suitable for the production of various ceramic materials. In addition, the presence of the diatom frustules with nanometric structures and the water absorption capability makes this material favorable for further use as absorption and filtration material.

Acknowledgment: The authors thank Professor Zlatko Levkov, Institute of Biology, Faculty of Natural Sciences, Ss. Cyril and Methodius University in Skopje, for his help during the process of identification and characterization of the frustules.

Funding information: The authors thank the financial support from the Ministry of Education and Science of North Macedonia and the Chemists Society of Turkey.

Author contributions: A. A. R.: conceptualization, investigation, methodology, writing – original draft, project administration, resources, visualization, and supervision; B. P.: conceptualization, project administration, writing – review and editing, supervision, and resources; E. F., A. B., M. P,. M. D., and C. S.: formal analysis and investigation; G. J.: investigation and writing – review and editing; P. M.: methodology, formal analysis, investigation, visualization, writing – review and editing, resources, and supervision; A. O.: formal analysis and resources.

Conflict of interest: The authors of this manuscript have no conflicts of interest to declare.

Data availability statement: The datasets generated during and/or analyzed during the current study are available from the corresponding author on rational request.

References

[1] Reka AA, Anovski T, Bogoevski S, Pavlovski B, Boškovski B. Physical-chemical and mineralogical-petrographic examinations of diatomite from deposit near village of Rožden. Republic of Macedonia Geologica Macedonica. 2014;28(2):121–6.
[2] Engh KR, editor. Diatomite. In: Kirk-Othmer encyclopedia of chemical technology. Hoboken, New Jersey: John Wiley & Sons, Inc; 2014. p. 55–9.
[3] Bakr H. Diatomite: its characterization, modifications and applications. Asian J Mater Sci. 2010;2(3):121–36. doi: 10.3923/ajmskr.2010.121.136.
[4] Calvert R. Diatomaceous earth. J Chem Edu. 1930;7(12):2829–49. doi: 10.1021/ed007p2829.
[5] Lutyński M, Sakiewicz P, Lutyńska S. Characterization of diatomaceous Earth and halloysite resources of Poland. Minerals. 2019;9(11):670. doi: 10.3390/min9110670.
[6] Smirnov PV, Konstantinov AO, Gursky HJ. Petrology and industrial application of main diatomite deposits in the Transuralian region (Russian Federation). Environ Earth Sci. 2017;76:682. doi: 10.1007/S12665-017-7037-3.
[7] Eldernawi AM, Rious JM, Al-Samarrai KI. Chemical physical and mineralogical characterization of Al-Hishal Diatomite at Subkhah Ghuzayil area Libya. Int J Res Appl Nat Soc Sci. 2014;2(4):165–74.
[8] Vu DH, Wang KS, Bac BH, Nam BX. Humidity control materials prepared from diatomite and volcanic ash. Constr Build Mater. 2013;38:1066–72. doi: 10.1016/j.conbuildmat.2012.09.040.
[9] Ediz N, Bentli İ, Tatar İ. Improvement in filtration characteristics of diatomite by calcination. Int J Miner Process. 2010;94(3–4):129–34. doi: 10.1016/j.minpro.2010.02.004.
[10] Yılmaz B, Ediz N. The use of raw and calcined diatomite in cement production. Cement Concrete Comp. 2008;30(3):202–11. doi: 10.1016/j.cemconcomp.2007.08.003.
[11] Janićijević J, Krajišnik D, Čalija B, Dobričić V, Daković A, Krstić J, et al. Inorganically modified diatomite as a potential prolonged-release drug carrier. Mater Sci Eng C Mater Biol Appl. 2014;42:412–20. doi: 10.1016/j.msec.2014.05.052.
[12] Ilia IK, Stamatakis MG, Perraki ThS. Mineralogy and technical properties of clayey diatomites from north and central Greece. Cent Eur J Geosci. 2009;1(4):393–403. doi: 10.2478/v10085-009-0034-3.
[13] Semenkova A, Belousov P, Rzhevskaia A, Semenkova A, Belousov P, Rzhevskaia A, et al. U(VI) sorption onto natural sorbents. J Radioanal Nucl Chem. 2020;36:293–301. doi: 10.1007/s10967-020-07318-y.
[14] Belousov P, Semenkova A, Egorova T, Romanchuk A, Zakusin S, Dorzhieva O, et al. Cesium sorption and desorption

on glauconite, bentonite, zeolite, and diatomite. Minerals. 2019;9(10):625. doi: 10.3390/min9100625.
[15] Akhtar F, Rehman Y, Bergström L. A study of the sintering of diatomaceous earth to produce porous ceramic monoliths with bimodal porosity and high strength. Powder Technol. 2010;201(3):253–7. doi: 10.1016/j.powtec.2010.04.004.
[16] Reka AA, Pavlovski B, Makreski P. New optimized method for low-temperature hydrothermal production of porous ceramics using diatomaceous earth. Ceram Int. 2017;43(15):12572–8. doi: 10.1016/j.ceramint.2017.06.132.
[17] Reka AA. Synthesis and characterization of porous SiO_2 ceramics obtained from diatomite with the use of low-temperature hydrothermal technology. PhD dissertation. Ss. Cyril and Methodius University, Skopje (MK); 2016.
[18] Manevich VE, Subbotin RK, Nikiforov EA, Senik NA, Meshkov AV. Diatomite – siliceous material for the glass industry. Glass Ceram. 2012;69:168–72. doi: 10.1007/s10717-012-9438-9.
[19] Yatsenko EA, Goltsman BM, Klimova LV, Yatsenko LA. Peculiarities of foam glass synthesis from natural silica-containing raw materials. J Therm Anal Calorim. 2020;142:119–27. doi: 10.1007/s10973-020-10015-3.
[20] Athar SD, Asilian H. Catalytic oxidation of carbon monoxide using copper-zinc mixed oxide nanoparticles supported on diatomite. J Health Scope. 2012;1:52–6. doi: 0.5812/jhs.4590.
[21] Inglethorpe SDJ. Industrial minerals laboratory manual: diatomite. Nottingham: British Geological Survey; 1993.
[22] Memedi H, Atkovska K, Lisichkov K, Marinkovski M, Kuvendziev S, Bozinovski Z, et al. Removal of Cr(VI) from water resources by using different raw inorganic sorbents. Quality of life. 2016;14(3–4):77–85. doi: 10.7251/QOL1603077M.
[23] Fragoulis D, Stamatakis MG, Papageorgiou D, Chaniotakis E. The physical and mechanical properties of composite cements manufactured with calcareous and clayey Greek diatomite mixtures. Cement Concrete Comp. 2005;27(2):205–9. doi: 10.1016/j.cemconcomp.2004.02.008.
[24] Rahimov RZ, Kamalova ZA, Ermilova EJO, Stojanov V. Thermally treated trepel as active mineral additive in cement. Gazette of Kazan Institute of Technology. 2014;17:99–101.
[25] Ibrahim SS, Selim AQ. Heat treatment of natural diatomite. Physicochem Probl Miner Process. 2012;48(2):413–24. doi: http://dx.doi.org/10.5277/ppmp120208.
[26] Loganina VI, Simonov EE, Jezierski W, Małaszkiewicz D. Application of activated diatomite for dry lime mixes. Constr Build Mater. 2014;65:29–37. doi: 10.1016/j.conbuildmat.2014.04.098.
[27] Zheng R, Ren Z, Gao H, Zhang A, Bian Z. Effects of calcination on silica phase transition in diatomite. J Alloys Comp. 2018;757:364–71. doi: 10.1016/j.jallcom.2018.05.010.
[28] Paules D, Hamida S, Lasheras RJ, Escudero M, Benouali D, Cáceres JO, et al. Characterization of natural and treated diatomite by laser-induced breakdown spectroscopy (LIBS). Microchem J. 2018;137:1–7. doi: 10.1016/j.microc.2017.09.020.
[29] Reza APS, Hasan AM, Ahmad JJ, Zohreh F, Jafar T. The effect of acid and thermal treatment on a natural diatomite. Chem J. 2015;1(4):144–50.
[30] Aguedal H, Hentit H, Merouani DR, Iddou A, Shishkin A, Jumas JC. Improvement of the sorption characteristics of diatomite by heat treatment. KEM. 2016;721:111–6. doi: 10.4028/www.scientific.net/kem.721.111.
[31] Reka A, Pavlovski B, Boev B, Boev I, Makreski P. Phase transitions of silica in diatomite from Besiste (North Macedonia) during thermal treatment. Proceedings of the II geology congress of Bosnia and Herzegovina, Geological society of Bosnia and Herzegovina, Laktaši, Bosnia and Herzegovin; 2019 Oct 2–4. p. 166–8.
[32] Reka AA, Pavlovski B, Anovski T, Bogoevski S, Boškovski B. Phase transformations of amorphous SiO_2 in diatomite at temperature range of 1000–1200°C. Geologica Macedonica. 2015;29(1):87–92.
[33] Reka AA, Pavlovski B, Ademi E, Jashari A, Boev B, Boev I, et al. Effect of thermal treatment of trepel at temperature range 800–1200°C. Open Chem. 2019;17:1235–43. doi: 10.1515/chem-2019-0132.
[34] Gulturk E, Guden M. Thermal and acid treatment of diatom frustules . J Achiev Mater Manuf Eng. 2011;46(2):196–203.
[35] Mineral commodity summaries 2020. Reston, Virginia: US Geological Survey; 2020. p. 56–7.
[36] Spasovski O, Spasovski D. The potential of the nonmetallic mineral resources in the Republic of Macedonia. Geologica Macedonica. 2012;26:91–4.
[37] Reka AA, Pavlovski B, Lisichkov K, Jashari A, Boev B, Boev I, et al. Chemical, mineralogical and structural features of native and expanded perlite from Macedonia. Geol Croat. 2019;72(3):215–21. doi: 10.4154/gc.2019.18.
[38] Cekova B, Pavlovski B, Spasev D, Reka A. Structural examinations of natural raw materials pumice and trepel from Republic of Macedonia. Proceedings of the XV Balkan Mineral Processing Congress, Sozopol, Bulgaria; 2013 Jun 12–16. p. 73–5.
[39] Pavlovski B, Jančev S, Petreski L, Reka A, Bogoevski S, Boškovski B. Trepel – a peculiar sedimentary rock of biogenetic origin from the Suvodol village, Bitola, R. Macedonia. Geologica Macedonica. 2011;25(1):67–72.
[40] Reka A, Pavlovski B, Boev B, Boev I, Makreski P. Chemical, mineralogical and structural characterization of diatomite from Republic of Macedonia. Proceedings of the 17th Serbian geological congress, Vrnjacka Banja, Serbia; 2018 May 17–20. p. 79–81.
[41] Reka AA, Durmishi B, Jashari A, Pavlovski B, Buxhaku NJ, Durmishi A. Physical-chemical and mineralogical-petrographic examinations of trepel from Republic of Macedonia. Int J Innov Stud Sci Eng Technol. 2016;2(1):13–7.
[42] Jovanovski G, Boev B, Makreski P. Minerals from the Republic of Macedonia with an introduction to mineralogy. Skopje, Macedonia: Macedonian Academy of Sciences and Arts; 2012.
[43] Spasovski O, Šijakova-Ivanova T, Doneva B, Spasovski D. New findings for diatomite (diatomaceous earth) between the villages of Manastir and Bešište (Mariovo). Geologica Macedonica. 2016;30(2):161–71.
[44] Gershanovski D, Jakjimovikj R. Determination of uranium and thorium content in some minerals from Mariovo, R. Macedonia, by k_0-instrumental neutron activation analysis. Physica Macedonica. 2001;51:35–42.
[45] Jovanovski G, Boev B, Makreski P, Najdoski M, Mladenovski G. Minerals from Macedonia XI. Silicate varieties and their localities – identification by FT IR spectroscopy. Bull Chem Technol Maced. 2003;22(2):111–41.

[46] Anthony JW, Bideaux RA, Bladh KW, Nichols MC, editors. Handbook of mineralogy: silica, silicates. Vol. 2 – Parts 1 & 2, Mineral Data Publ; 1995.
[47] Lafuente B, Downs RT, Yang H, Stone N. The power of databases: the RRUFF project. In: Armbruster T, Danisi RM, editors. Highlights in mineralogical crystallography. Berlin, Germany: W. De Gruyter; 2015. p. 1–29.
[48] Chen F, Miao Y, Ma L, Zhan F, Wang W, Chen N, et al. Optimization of pore structure of a clayey diatomite. Particul Sci Technol. 2019;38(5):522–8. doi: 10.1080/02726351.2019.1567635.
[49] Krupskaya V, Novikova L, Tyupina E, Belousov P, Dorzhieva O, Zakusin S, et al. The influence of acid modification on the structure of montmorillonites and surface properties of bentonites. Appl Clay Sci. 2019;172:1–10. doi: 10.1016/j.clay.2019.02.001.
[50] Memedi H, Atkovska K, Lisichkov K, Marinkovski M, Kuvendziev S, Bozinovski Z, et al. Separation of Cr(VI) from aqueous solutions by natural bentonite: equilibrium study. Quality of Life. 2017;15(1–2):41–7. doi: 10.7251/QOL1701041M.
[51] Chukanov NV. Infrared spectra of mineral species. Dordrecht, Netherlands: Springer Geochemistry/Mineralogy; 2014.
[52] Chaisena A, Rangsriwatananon K. Effects of the thermal and acid treatments on some physico-chemical properties of Lampang diatomite. Suranaree J Sci Technol. 2004;11(4):289–99.
[53] Mohamedbakr H, Burkitbaev M. Elaboration and characterization of natural diatomite in Aktyubinsk/Kazakhstan. Open Mineral J. 2009;3:12–6.
[54] Tironi A, Trezza MA, Irassar EF, Scian AN. Thermal treatment of kaolin: effect on the pozzolanic activity. Proc Mater Sci. 2012;1:343–50.
[55] Holt JB, Cutler IB, Wadsworth ME. Rate of thermal dehydration of muscovite. J Am Ceram Soc. 1958;41(7):242–6. doi: 10.1111/j.1151-2916.1958.tb13548.x.
[56] Ognjanova-Rumenova N, Jovanovska E, Cvetkoska A, Levkov Z. Two new Tertiarius (Bacillariophyta, Coscinodiscophyceae) species from Mariovo Neogene Basin, Macedonia. Fottea. 2015;15(1):51–62.
[57] Memedi H, Atkovska K, Kuvendziev S, Garai M, Marinkovski M, Dimitrovski D, et al. Removal of Chromium(VI) from aqueous solution by clayey diatomite: kinetic and equilibrium study. In: Stafilov T, Balabanova B, editors. Contaminant levels and ecological effects – understanding and predicting with chemometric methods, Springer, Switzerland; 2021. p. 263–82. doi: 10.1007/978-3-030-66135-9_9.
[58] Ruggiero I, Terracciano M, Martucci NM. Diatomite silica nanoparticles for drug delivery. Nanoscale Res Lett. 2014;9:329. doi: 10.1186/1556-276X-9-329.
[59] Issi A. Estimation of ancient firing technique by the characterization of semi-fused Hellenistic potsherds from Harabebezikan/Turkey. Ceram Int. 2012;38(3):2375–80. doi: 10.1016/j.ceramint.2011.11.002.